aerospace

MDPI

Article

A Study on a Vitiated Air Heater for a Direct-Connect Scramjet Combustor and Preliminary Test on the Scramjet Combustor Ignition

Jae-Hyuk Lee, Eun-Sung Lee, Hyung-Seok Han, Min-Su Kim and Jeong-Yeol Choi *

Department of Aerospace Engineering, Pusan National University, Busan 46241, Republic of Korea
* Correspondence: aerochoi@pusan.ac.kr

Abstract: Vitiation air heater (VAH) combustion characteristics for a direct-connect scramjet combustor (DCSC) were experimentally studied. The VAH consists of a head, modular chamber, and circular-to-rectangular shape transition (CRST) nozzle. The CRST nozzle transforms the circular cross-sectioned rocket-type VAH into a rectangular cross-sectioned scramjet combustor. The CRST nozzle exit Mach numbers at the top, middle, and bottom were measured using a tungsten wedge. The oblique shock formed by the wedge was captured using Schlieren visualization and recorded with a high-speed camera. The θ-β-M relation showed that the exit Mach number was 2.04 ± 0.04 with a chamber pressure of 1.685 ± 0.07 MPa. With the VAH design point verified, preliminary scramjet combustor ignition tests were conducted. As the fuel was not auto-ignited by the vitiated air, the forced ignition method, in which VAH ignition flame ignites the scramjet fuel, was used. The Schlieren images showed that a cavity shear layer combustion mode was formed and also showed that the forced ignition method could be used as a reference model for the ignitor-ignition method.

Keywords: vitiated air heater; direct-connect scramjet combustor; scramjet combustor; rocket type combustor

Citation: Lee, J.-H.; Lee, E.-S.; Han, H.-S.; Kim, M.-S.; Choi, J.-Y. A Study on a Vitiated Air Heater for a Direct-Connect Scramjet Combustor and Preliminary Test on the Scramjet Combustor Ignition. *Aerospace* **2023**, *10*, 415. https://doi.org/10.3390/aerospace10050415

Academic Editor: Jian Liu

Received: 27 February 2023
Revised: 16 April 2023
Accepted: 24 April 2023
Published: 28 April 2023

1. Introduction

A ground test of a hypersonic propulsion system requires a high-enthalpy air supply system. A heat generation facility is necessary to generate high-enthalpy air. The facility can be categorized into continuous, pulse, and blowdown types, as shown in Table 1. The continuous type provides continuous airflow produced by a compressor. However, as the cost per test is prohibitive, the facility is constructed in a few selective institutes. Liu et al. optically investigated an axisymmetric scramjet in a pulsed arc heater supersonic combustion tunnel [1]. The arc heater produced high-enthalpy, high-Mach number freestream airflow at a Mach number of 4.5, a total temperature of 2200 K, a total pressure of 0.160 MPa, and a test duration of one second. The results of a scramjet investigation study utilizing this type of facility showed that the cavity flameholder created a recirculation zone, a shear layer, and a recompression shock that interacted with the flowing mixture to stabilize the flame and improve combustion. Furthermore, flames resided inside the shear layer region above the cavity and piloted the combustion at the diverging combustor. Although there are facilities that can obtain meaningful results such as these, they require high costs and are difficult to build. The ACT-2 used in this study is powered by a 250 kW Magna Power Series M unit to provide voltage up to 600 V and current up to 400 A [2]. Regarding the pulse type of the facility, the operation condition is different to the continuous type. The construction and test costs are low with a few microseconds of operation time. However, due to insufficient operation time, steady-state combustion is difficult to achieve. Vanyai et al. investigated a scramjet combustor in a T4 free-piston shock tunnel at The University of Queensland. The shock tube provided supersonic airflow at a Mach number of 3.8, a temperature of 668–832 K, and a static pressure of 32.8–33.7 kPa [3]. Through this shock

tube facility, it was possible to show that the pressure rise due to combustion is significant when the equivalence ratio is 0.3 or more. Additionally, radicals representing a reaction zone were typically found in thick annular rings between the likely combustion products at the walls and the fuel-lean core flow. However, in a study by Jeong et al. using the same type of facility, the total test time for static pressure measurement was 1.25–1.75 ms, which was 0.5 ms, and the laser for PLIF imaging was triggered at 1.5 ms. As a result, it can be seen that there is a drawback insofar as a very short test time is allowed [4].

Table 1. Comparison of air heat generation facilities.

Facility Type	Continuous	Pulse	Blowdown	
Heat generation	Compressor	Pressure/ temperature rise via shock compression	Air vitiation	Combustion (combustion product)
				Electric heating (air dissociation)
				Heat accumulation (particulates)
Operation-time	Continuous	Order of 10 ms	Order of seconds	
Cost	Very high	Low	Low	

The blowdown-type heat-generation facility creates vitiated air adequate for a lab-scale direct-connect scramjet combustor facility. The molar composition, enthalpy, and pressure of vitiated air are determined by the fuel and oxidizer used to heat the air. The operation time is an order of seconds, and the cost per test is low, minimizing the facility size. Abundant experimental studies have used a blowdown-type facility. An aerodynamic and propulsion test unit (APTU) was constructed and tested by Garrard et al. The APTU produced vitiated air using a butane and liquid oxygen sudden-expansion burner and provided a Mach number of 4.5, a total pressure of 2.07 MPa, a total temperature of 1111 K, and 12 min of test duration [5]. Meng et al. constructed a variable Mach number direct-connected supersonic combustor test facility using a heater. The heater combusted hydrogen, oxygen, and air and provided a Mach number of 2.4–2.9, a total pressure of 1.47–1.98 MPa, a total temperature of 1228–1686 K, and mass flow rate of 1.076–1.795 kg/s. The facility used in this experimental study has a heating preparation time of 14 s, followed by an ignition time of about 1.5 s to form an inflow condition. There is a feature that requires a relatively long preparation time [6]. Zhang et al. tested a kerosene-fueled supersonic combustor at a directly connected scramjet combustor test rig. The air heater burning ethanol and oxygen fed a high-enthalpy air flow at a Mach number of 2.8 through a Laval nozzle. In this study, after the heated air flow is stable, the plasma torch ignitor and injection of liquid kerosene begins. Through this method, the interaction between combustion and flowing can be analyzed experimentally and numerically. It was determined that the diffusion and the propagation of the flame affect the flowing field characteristic, inducing boundary layer separation and enlarging the subsonic region to further improve the flame propagation process. In addition, the flashback mechanism of both the core flame and the wall flame was revealed [7]. Peng et al. tested the combustion instability of a scramjet combustor using a direct-connect supersonic combustion facility. The vitiated air heater provided high-enthalpy air flow by heating a hydrogen–air mixture. The airflow was supplied at a Mach number of 2.20 at the isolator inlet, a total temperature of 950 K, and a total pressure of 0.8 MPa. It took 0.26 s to form vitiated air of constant pressure, and hydrogen fuel was injected into the combustor immediately after. The vitiated air flow entering the test article had a molar composition of 21% O_2, 12% H_2O, and 67% N_2 and a mass flow rate of 2.68 kg/s and was called vitiated air because of an H_2O admixture. Using the high-speed OH-PLIF technique and DMD analysis, it was found that the oscillations at 80–120 Hz were remarkably enhanced due to the positive growth factors in ram-to-scram

transition. As the equivalence ratio of hydrogen increased, low-frequency oscillations could be found [8,9]. In addition to this, numerous scramjet combustion tests through vitiated air supply have been performed. Nishimoto et al. investigated the penetration height of an ethylene jet in a supersonic crossflow using a supersonic combustion ramjet model. The vitiated air heater using hydrogen, oxygen, and air provided supersonic airflow at a Mach number of 2, a total temperature of 1900 K, and a total pressure of 0.37 MPa [10]. Wang et al. investigated the low-frequency oscillation of an ethylene-fueled supersonic combustor at a direct-connect test facility. The air heater burning pure alcohol and oxygen provided vitiated air at a Mach number of 2.1, a total temperature of 846 K, a total pressure of 0.76 MPa, and a total mass flow rate of 2.02 kg/s [11]. Yuan et al. investigated flame stabilization modes in a supersonic combustor in a direct-connect supersonic combustor. The vitiated air supply system supplied vitiated air at a Mach number of 2.5, a total temperature of 1200–1800 K, and a total pressure of 1.0 MPa [12]. Zhang et al. investigated flame liftoff characteristics in a supersonic combustor in a ground-directed test rig. An vitiation air heater using ethanol and oxygen provided vitiated air at a Mach number of 2.8, a total temperature of 1680 K, and a total pressure of 1.87 MPa [13]. Li et al. investigated flame stabilization in a scramjet combustor in a direct-connected test facility. The air heater heated the air via ethanol and oxygen combustion, providing vitiated air at a Mach number of 2.1, a total temperature of 947 K, a total pressure of 0.71 MPa, and a total mass flow rate of 2 kg/s [14]. An et al. studied the flame stabilization enhancement in a scramjet combustor with shock wave generators at a direct-connect test facility. The air heater produced high-enthalpy air by burning C_2H_6O, oxygen, and air and fed vitiated air at a Mach number of 2.92, a total temperature of 1650 K, a total pressure of 2.6 MPa, and a total mass flow rate of 1 kg/s [15]. Nakaya et al. investigated combustion instability in a scramjet combustor in a supersonic combustion ram jet model combustor. The vitiated heater burning hydrogen and oxygen supplied vitiated air at a Mach number of 2, a total temperature of 1900 K, and a total pressure of 0.37 MPa [16]. Yang et al. experimentally investigated the effect of injection structures using a direct-connected test platform at the National University of Defense Technology in China. The air heater heated air using ethanol, oxygen, and air, providing vitiated air at a Mach number of 2.4, a total temperature of 1500 K, a total pressure of 1.1 MPa, and a total mass flow rate of 1 kg/s [17].

In the study of numerical analysis, efforts were made to simulate the environment of a real scramjet as closely as possible. Since non-uniform flow occurs throughout the scramjet in areas such as the isolator, combustor, and nozzle, an integrated design method was proposed based on the method of characteristics (MOC) to generate flow distortion through shock wave interaction, in order to account for this phenomenon [18].

In this study, a vitiation air heater (VAH) for a direct-connect scramjet combustor (DCSC) was manufactured and tested. The VAH heated and supplied vitiated air through combustion via a chemical reaction, and the target corresponded to a flight Mach number of 4.0 to 5.0 and an altitude of 20 to 25 km. It does not require a high-power device like the arc-heater method, and it can achieve a sufficient operating time corresponding to an order of seconds and is thus a low-cost facility suitable for lab-scale. The mole fraction of vitiated air corresponds to 21% O_2, 20.5% H_2O, and 58.5% N_2. A remote-controlled monitoring system was constructed for fully automatic and remote experiments. The Mach number at the exit of the nozzle was measured using a wedge, and Schlieren flow visualization was achieved with a high-speed camera. The preliminary tests for scramjet ignition and combustion were conducted.

2. Experimental Apparatus

2.1. Vitiation-Air-Heater Experimental Model

The DCSC used in this study is depicted in Figure 1. The DCSC consists of a VAH, an isolator, and a scramjet combustor. The target design points of the VAH exit were designed to match the flight conditions of a Mach number of 4.0–5.0 and flight altitude of 20–25 km. The VAH conditions were calculated using the NASA CEA code [19] and isentropic relation:

The exit condition was a Mach number of 2.0, the stagnation pressure was 0.226 MPa, and the stagnation temperature was 1000 K. Through this, an inlet condition corresponding to a total pressure of 1.732 MPa and a total temperature of 1578 K can be derived. The VAH design was based on a rocket-type combustor model designed by Marshall et al. [20]. The VAH consists of a head, a modular chamber, and a circular-to-rectangular transition (CRST) nozzle. Room-temperature gaseous hydrogen (GH_2) and gaseous oxygen (GO_2) are injected through a shear coaxial injector installed at the head, as illustrated in Figure 2. The head is made of stainless steel (SUS303) and is 100 mm long. For the film-cooling effect, the air was injected along the inner wall of the chamber through 24-hole injectors with a diameter of 1.5 mm. The chamber of the VAH was manufactured in modular type, which can be changed according to combustion characteristics. Each chamber module has a 30 mm wall thickness, 40 mm inner diameter, and 100 mm length, which is made of oxygen-free copper (C102) to endure hydrogen embrittlement and ablation. The CRST nozzle was designed for optimal cross-section transition and uniform flow feed based on the method of characteristics. The subsonic section does not have a significant effect on the flow field after the throat, as shown in Figure 3. Therefore, as shown in Figure 4 and Table 2, the geometric design variables of the upstream section of the nozzle throat were defined and designed. The design process was covered in detail in a study by Sung et al. [21,22]. The nozzle has a 130 mm length, a Ø 40 mm inlet, and a 20 × 20 mm rectangular outlet. Flanges were used to connect the chamber, nozzle, and isolator. Between each component, metal (C122) and rubber (Viton) o-rings were installed for sealing.

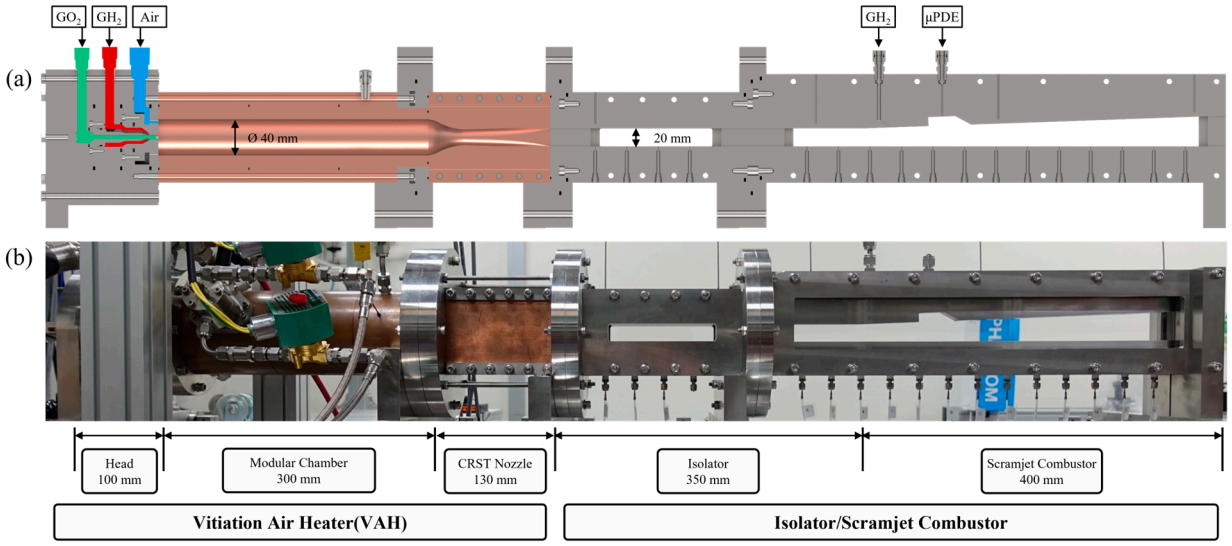

Figure 1. Schematics of the direct-connect scramjet combustor. (**a**) CAD schematics. (**b**) Experimental model.

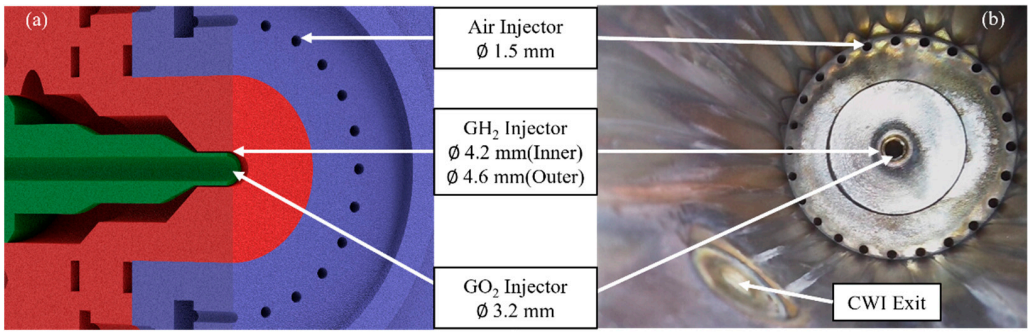

Figure 2. VAH head shear coaxial GH_2/GO_2 injector. (**a**) CAD model. (**b**) Experimental model.

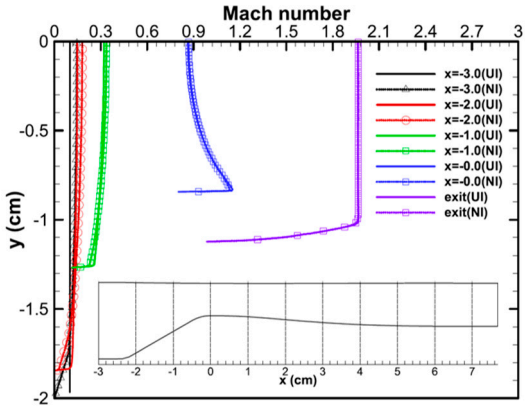

Figure 3. Inflow Mach number distribution and the corresponding exit Mach number distribution without boundary layer correction. UI and NI stand for uniform inflow and non-uniform inflow, respectively [22].

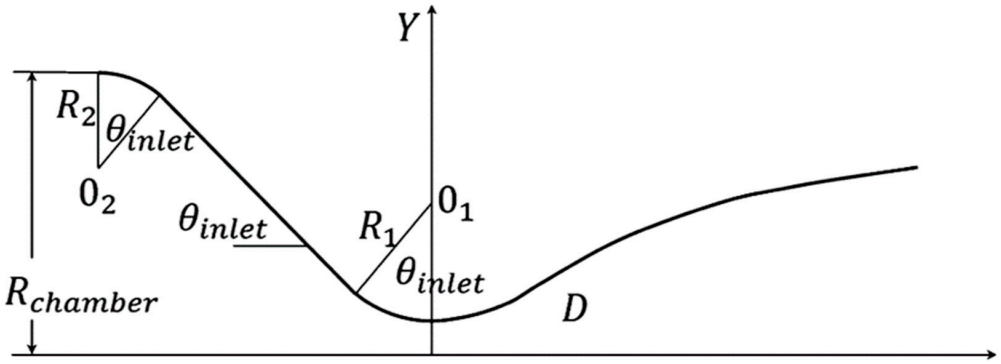

Figure 4. Geometric features of contraction section [21].

Table 2. Geometric features of converging section of the nozzle (dimensions in mm).

$R_{chamber}$	R_1	R_2	Θ_{inlet}
20.0	10.0	5.0	30°

A combustion wave ignitor (CWI) was used to ignite the VAH, which was based on the model designed by Han et al. [23]. The CWI was installed at the chamber wall 50 mm from the VAH head, as shown in Figure 5. The combustion channel had a Ø 20 mm circular cross-section and 125 mm length and was made of SUS304. The fuel and oxidizer were identical to the VAH, with a mass flow rate of 1.02 g/s and an equivalence ratio of 1.04. The propellant feeding was controlled using solenoid valves, which were opened for 0.1 s. A spark plug was used to ignite the CWI, and activation frequencies were regulated using a pulse width modulation circuit. The preliminary tests for CWI were conducted. The Schlieren image was captured using a high-speed camera (Phantom Inc., Wayne, NJ, USA) recording at a resolution of 1280 × 800, sampling rate of 25,000 fps, and exposure of 7.0 µs. The Schlieren and digital camera snapshots showed that the plume length was 10 cm, propagating in 20 ms with shockwaves, sufficiently covering the VAH chamber. Figure 6 shows the operating mechanism of CWI. In these preliminary tests, the mixture of GH_2 and GO_2 was all filled within 5 ms. Between 16.8 and 16.9 ms, the spark plug was ignited, and the shock wave and plume were ejected accordingly. Following this, the plume was propagated and maintained until the solenoid valve closed. By designing, manufacturing, and utilizing the CWI proposed in this study, no expensive additional devices are required for VAH operation.

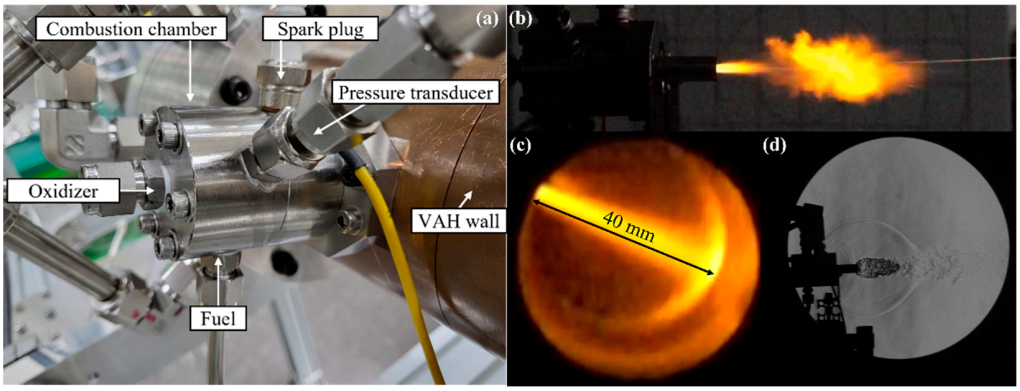

Figure 5. (**a**) CWI installation and CWI preliminary tests. (**b**) Digital camera snapshot. (**c**) CWI flame length covering VAH chamber. (**d**) Schlieren snapshot.

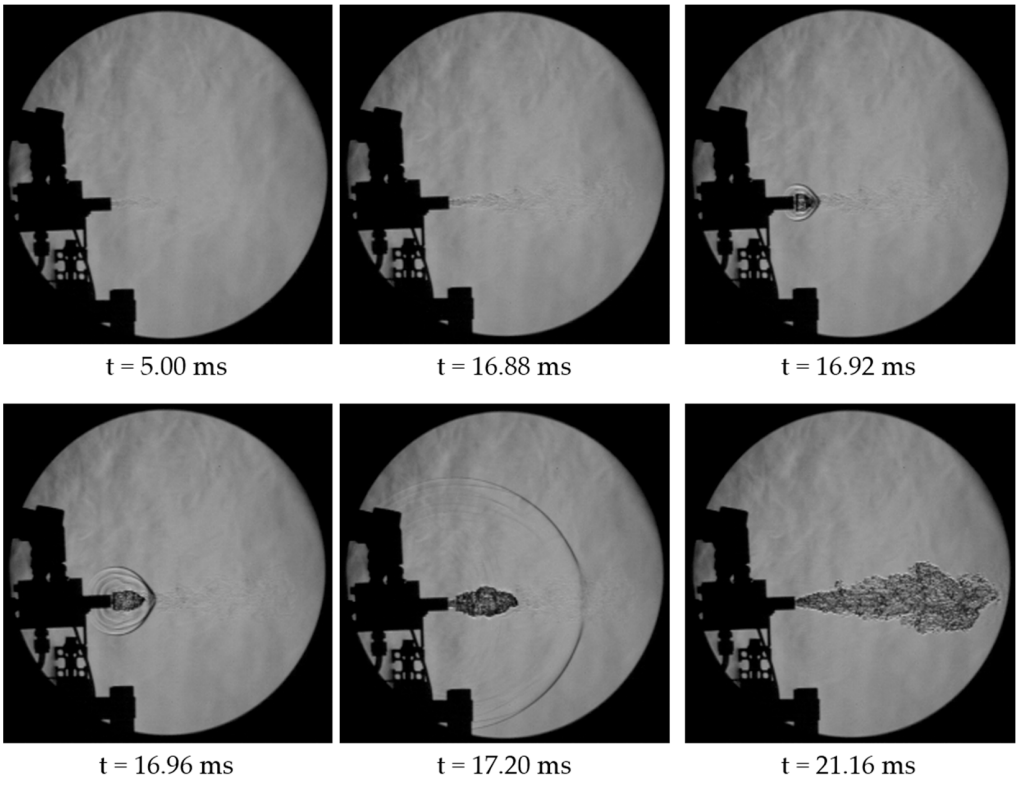

Figure 6. Schlieren instantaneous images of CWI operation.

2.2. Gas Supply System

The target VAH nozzle outlet conditions included a Mach number of 2.0, a stagnation temperature of 1000 K, and a stagnation pressure of 0.226 MPa, corresponding to a total mass flow rate of 368.25 g/s calculated through isentropic relation assuming an inviscid, incompressible, and steady-state fluid. The injection pressure and mass flow rate of each gas were determined based on the chemical equation of a choked nozzle. The gas supply system consists of an external gas clustering facility and an internal high-pressure gas supply system, as shown in Figure 7. The external gas clustering facility clustered and supplied each gas to the test compartment, as shown in Figure 8. As air especially required a high mass flow rate, 25 cylinders of 40 L were clustered and fed through a 1-inch tube. Five cylinders of GH_2 and GO_2 were clustered in separate compartments. In the case of GN_2, there were five cylinders clustered: four cylinders were used for purge and valve control, while the other was used for regulator control. Gas-leak-detection sensors and relief valves were installed to detect leakage and prevent pressure surges.

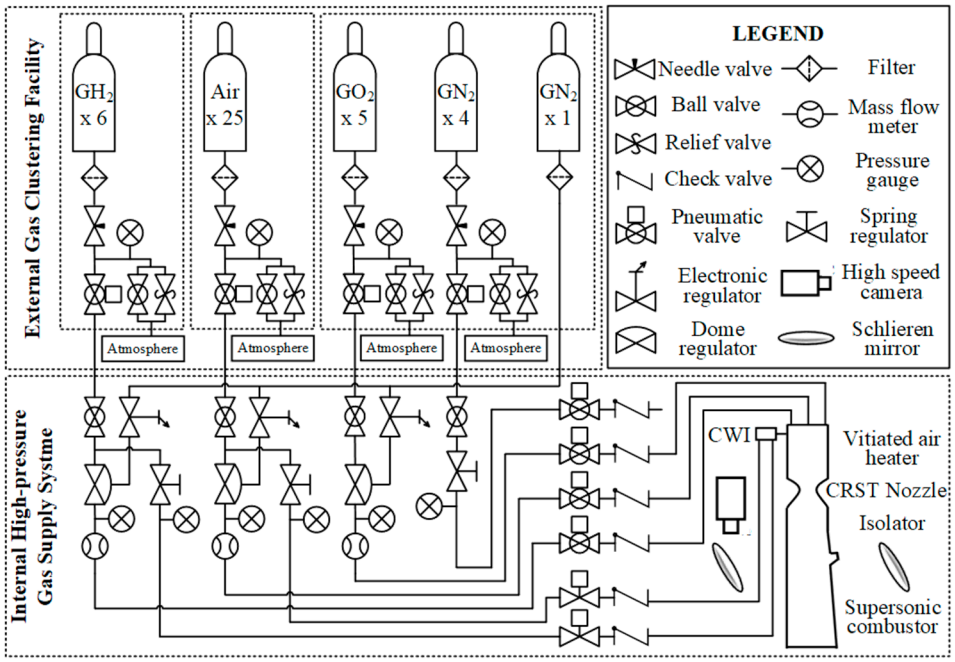

Figure 7. DCSC piping and instrumentation drawing.

Figure 8. External (**a**) air, (**b**) GH_2, (**c**) GO_2, and (**d**) GN_2 clustering compartments.

As shown in Figure 7, in the internal high-pressure gas supply system, the dome regulators (Swagelok Inc., RDHN series, Solon, OH, USA) controlled by electronic regulators (ProportionAir Inc., GX series, Mccordsville, Indiana) enabled precise pressure control of GH_2, GO_2, and air. Spring regulators (Swagelok Inc., KPR series, Solon, OH, USA) were installed to control the GN_2, which does not require acute pressure control. Each supply line was equipped with a pressure differential mass flow meter (Enbac Inc., FM153B, Republic of Korea, <0.2% FS sensor accuracy). Pneumatic valves (Swagelok Inc., AT series, Solon, OH, USA) with solenoid valves (Emerson Inc., ASCO 551 series, Florham Park, NJ, USA) controlled flow according to the sequence. Pressure transmitters (WIKA Inc., S-20 series, Germany, <0.5% sensor error) were used to measure the pressure of plenums, cluster tubes, and regulated pressure. The thermocouples (Omega Inc., K-type, Norwalk, CT, USA) measured the temperature of VAH exit. Thrust was measured using an S-Beam type load cell (CAS Inc., Seoul, Republic of Korea, SBA series).

2.3. Remote Control and Monitoring System

A remote-controlled monitoring system was constructed using LabVIEW and the CompactRIO module to acquire and save data. As shown in Figure 9, real-time valve control, flow and pressure control, and data acquisition were performed. Figure 10 shows the control computer, safety switches, and LabVIEW switchboard.

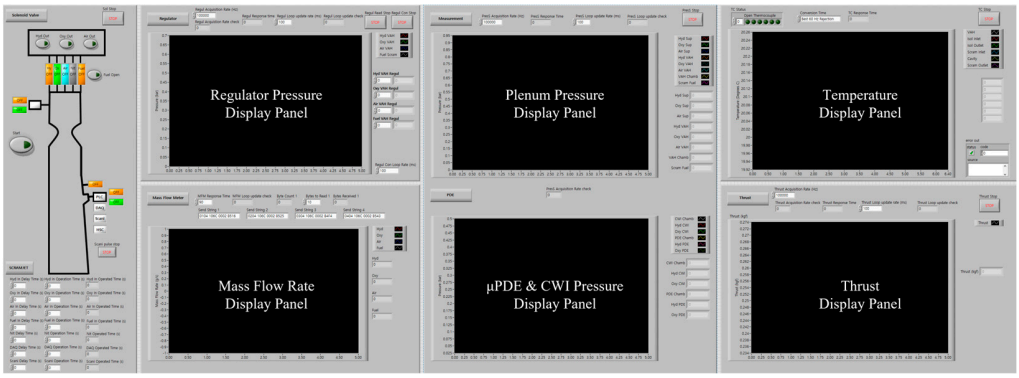

Figure 9. Remote-controlled monitoring system panel for the DCSC experiment.

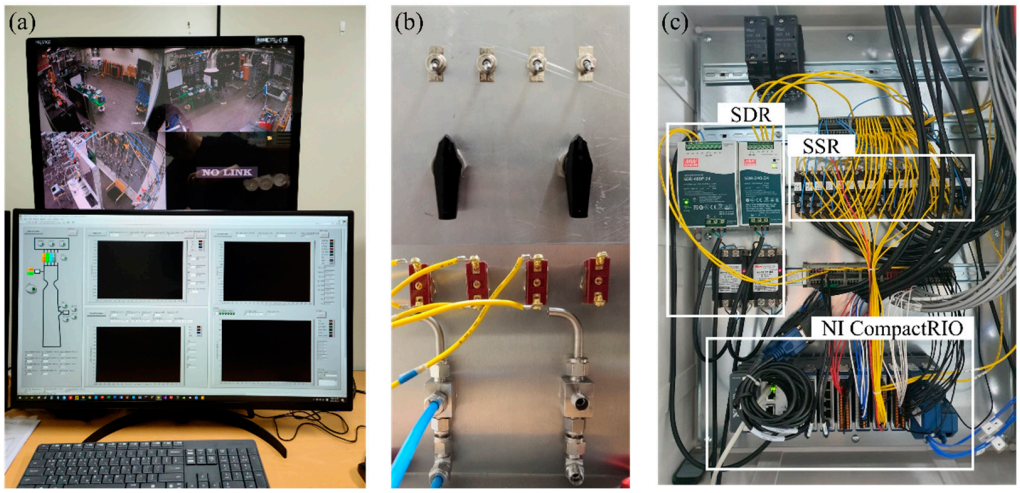

Figure 10. (**a**) Controller computer and CCTV, (**b**) Safety Switch, and (**c**) CompactRIO switchboard.

Table 3 shows the modules and their control devices. The test can be forcefully terminated in an emergency by shutting down the safety switch. The solenoid state relays controlled the valves and spark plugs according to the sequence.

Table 3. CompactRIO 9045 controller modules.

Module	Signal Type	Control
NI9871	RS485	Mass flow meter
NI9205	Voltage input	Pressure transmitter
NI9263	Voltage output	Electronic regulator
NI9375	Digital input/output	Solenoid valve
NI9212	Thermocouple input	Thermocouple
NI9401	TTL	High-speed camera, Scanivalve

3. Results and Discussion

3.1. Preliminary Test

Preliminary tests were conducted to set the VAH ignition sequence. When the targeted mass flow rate was fed into the plenum, there was a 20–30% pressure loss compared to the theoretical expectations. The pressure of each plenum showed a steady state within 0.7 s. When GH_2, GO_2, and air were supplied simultaneously, thanks to the film cooling effect of air, CWI could not ignite the VAH. Therefore, the CWI ignited when the plenum of GH_2 and GO_2 reached a steady state, as shown in Figure 11. The air was supplied after the VAH ignition. The combustion lasted for one second. The combustion terminated with GN_2 purge.

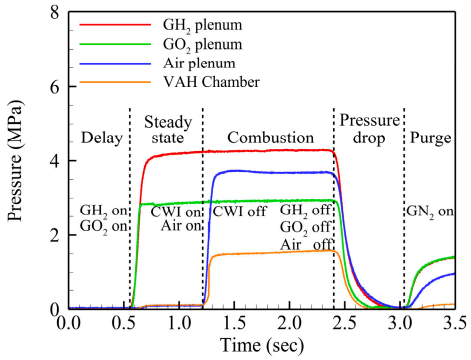

Figure 11. Static pressure history of VAH plenum and chamber.

3.2. Exit Mach Number Measurement: P_c = 0.789 MPa

The exit Mach numbers at the top, middle, and bottom were measured based on the θ-β-M relation, as shown in Equation (1). The design pressure of the VAH was 0.226 MPa, which was expected to create expansion shocks at the top and bottom. Therefore, as the exit Mach number is a function of an area ratio (Equation (2)) the Mach numbers were measured at an exit pressure of 0.1 MPa, which did not form expansion shocks at the exit. The specific heat ratio γ applied to Equations (1) and (2) is 1.29 [22].

$$\tan\theta = 2\cot\beta\frac{M_1^2\sin^2\beta - 1}{M_1^2(\gamma + \cos 2\beta) + 2} \tag{1}$$

$$\frac{A}{A^*} = \left(\frac{\gamma+1}{2}\right)^{\frac{-(\gamma+1)}{2(\gamma-1)}}\frac{1}{M}\left(1 + \frac{\gamma-1}{2}M^2\right)^{\frac{\gamma+1}{2(\gamma-1)}} \tag{2}$$

Figure 12 shows the wedges used for this study. The stainless steel, graphite, and copper wedges ablated due to the high-enthalpy vitiated air at the CRST nozzle exit. The tungsten wedges were installed and showed minor deformation. However, as the 10° leading edge ablated within 10 test cycles, 15° and 20° were used.

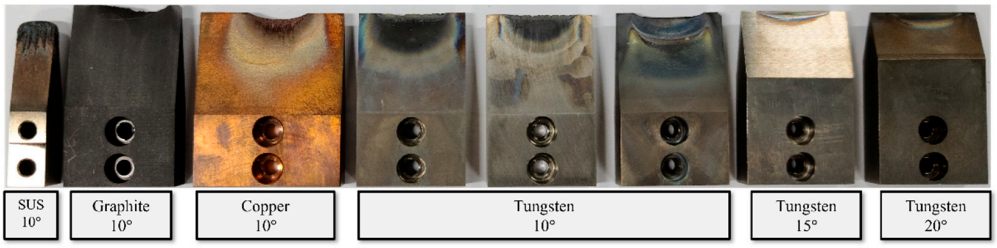

Figure 12. Mach number measurement wedges.

Figure 13 shows the Schlieren snapshots at the VAH exit with the wedges installed at the top, middle, and bottom, where the chamber pressure was 0.789 ± 0.06 MPa. The images were enhanced by +40% brightness and +40% contrast. It was performed 2–3 times for repeatability, and the Mach numbers and chamber pressure are shown in Table 4. As the oblique shock angles were measured by hand, the measurement took more than five attempts to minimize the error. Before measurement, the measurement function of PCC v3.7 software was used to calibrate the Schlieren images, which correspond to 0.177 mm/pixel. The Mach numbers at the top, middle, and exit showed little difference and matched the theoretical target. A thermocouple was installed at the VAH exit. As the thermocouple was exposed to the high-enthalpy fluid and had a slow response time, it was difficult to find thermal characteristics around the exit. The temperature profile ranged from 1047.75 K to 1376.55 K.

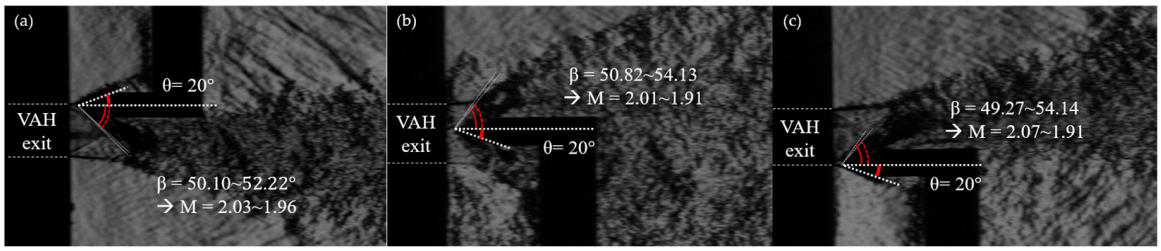

Figure 13. Schlieren snapshot at the (**a**) top, (**b**) middle, and (**c**) bottom of the CRST nozzle exit, where $P_c = 0.765 \pm 0.061$ MPa.

Table 4. Experimental and theoretical result for $P_c = 0.789 \pm 0.06$ MPa.

		Experiment	Theory
Mass Flow Rate (g/s)	GH_2	1.72 ± 0.61	2.52
	GO_2	29.74 ± 0.74	30.58
	Air	124.92 ± 7.27	129.99
P_c (MPa)		0.789 ± 0.06	0.765
Mach	Top	2.02 ± 0.03	
	Middle	2.00 ± 0.01	2
	Bottom	2.02 ± 0.01	

The boundary layer thickness and exit Mach number were measured at the isolator exit. Figure 14 shows the boundary layer thicknesses at the top and bottom developed to 2.8 mm and 4.2 mm, respectively. As the boundary layer reduced the effective flow area, the flow decreased to Mach 1.85 ± 0.1, as shown in Figure 15. Figure 16 shows the bow shocks formed at the top and bottom of the isolator due to the effect of the boundary layer.

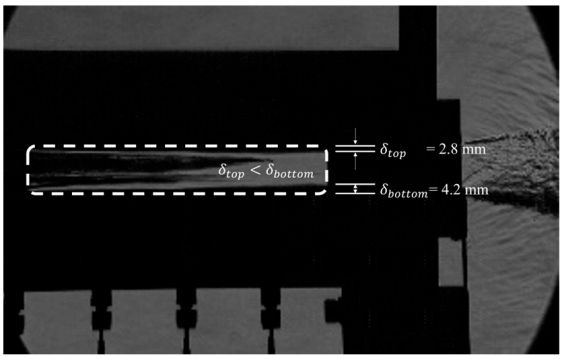

Figure 14. Schlieren snapshot of isolator boundary layer, where $P_c = 0.765 \pm 0.061$ MPa.

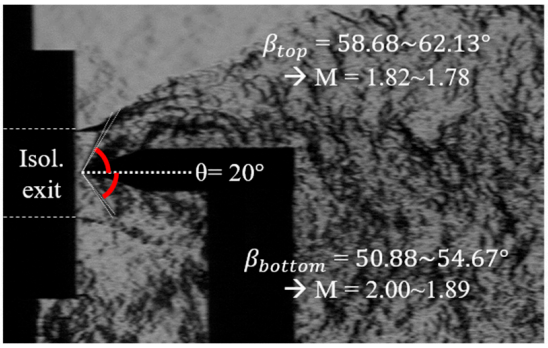

Figure 15. Schlieren snapshot at the middle of isolator exit, where $P_c = 0.765 \pm 0.061$ MPa.

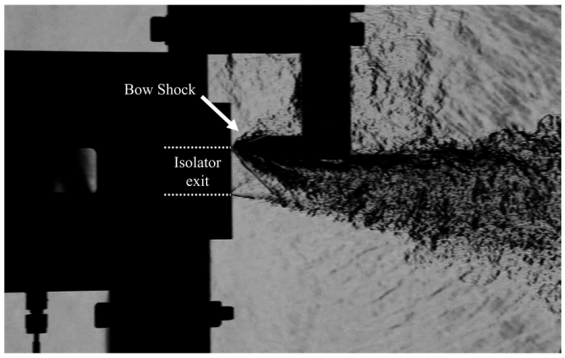

Figure 16. Schlieren snapshot at the top of isolator exit, where P_c = 0.765 ± 0.061 MPa.

3.3. Design Verification Test Result

Figure 17 shows the Schlieren snapshot, where the chamber pressure was 1.685 ± 0.07 MPa. The Mach number at the middle was 2.04 ± 0.04, while it could not be measures at the top and bottom due to expansion shock. Table 5 compares the experimental results and theoretical targets. The differences in the mass flow rate, chamber pressure, and Mach number were presumably due to the irreversibility of the VAH. In addition, motor scale measurement and comparison with theoretical calculation values were performed using the S-Beam type load cell, as shown in Table 6. Furthermore, three additional combustion tests were conducted for repeatability.

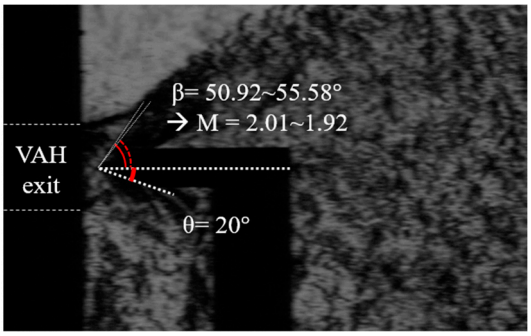

Figure 17. Schlieren snapshot at the middle of the CRST nozzle exit, where P_c = 1.685 ± 0.072 MPa.

Table 5. Experimental and theoretical result for P_c = 1.685 ± 0.072 MPa.

		Experiment	Theory
Mass Flow Rate (g/s)	GH_2	4.88 ± 0.53	5.68
	GO_2	68.84 ± 0.25	69.04
	Air	288.39 ± 11.38	293.52
P_c (MPa)		1.685 ± 0.07	1.727
Mach	Middle	2.04 ± 0.04	2

Table 6. Experimental and theoretical result of motor scale.

P_c (MPa)	Experimental Max. Thrust (N)	Theoretical Thrust (N)
1.661	518.30	515.38
1.654	513.31	
1.646	510.25	

The theoretical design thrust is calculated by using Equation (3) with the values presented as the target design conditions of the VAH exit.

$$F = \dot{m}V_e + (P_e - P_0)A_e \quad (3)$$

3.4. Scramjet Combustor Preliminary Test: Forced Ignition

In actual flight conditions, the fuel is injected after the air passes through the combustor. In this study, however, as the fuel, room-temperature GH_2 was not auto-ignited by the vitiated air, and thus an ignitor was required. Before further ignitor study was conducted, the forced ignition method was used, wherein VAH ignition energy ignited the scramjet fuel. Figures 18 and 19 show the forced ignition sequence. (1) The pneumatic valves of GH_2 and GO_2 were opened, and plenum pressure started to rise. (2) As the plenum pressure reached a steady state, the CWI was ignited. Simultaneously, the scramjet fuel was injected into the scramjet combustor. The high-temperature combustion from the VAH ignited the scramjet fuel. (3) The air was fed into the VAH, and vitiated air was generated. The scramjet combustor started steady combustion. (4) The scramjet fuel feed was cut off while vitiated air was supplied into the scramjet combustor. (5) The test terminated as the VAH gas supply valve closed. The room-temperature GN_2 was supplied for purge.

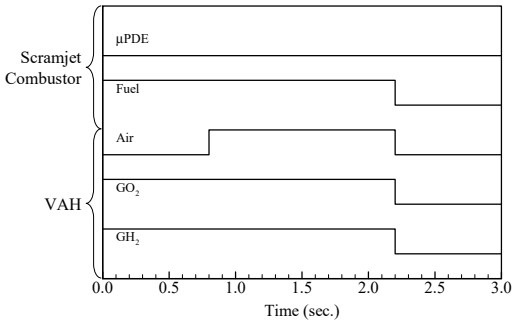

Figure 18. Forced ignition sequence schematic.

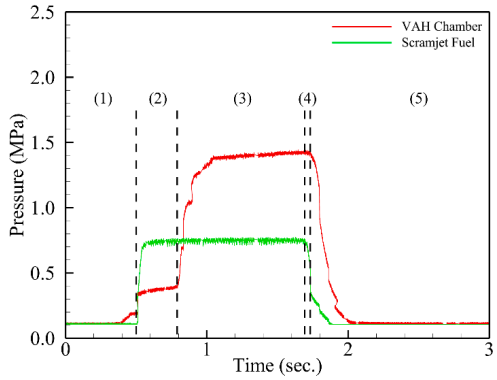

Figure 19. Forced ignition of scramjet combustor using VAH ignition energy.

Figure 18 is the valve control sequence for forced ignition, and the pressure was formed according to the time sequence as shown in Figure 19.

Figure 20 shows the wall pressure history along the isolator and scramjet combustor, where the combustor inlet was set to x = 0. When scramjet fuel was not supplied, vitiated air pressure decreased along the channel. The maximum pressure below the cavity was 0.19 MPa. Therefore, an ignitor, such as a micro-pulse detonation engine, should provide higher pressure than vitiated air under the cavity.

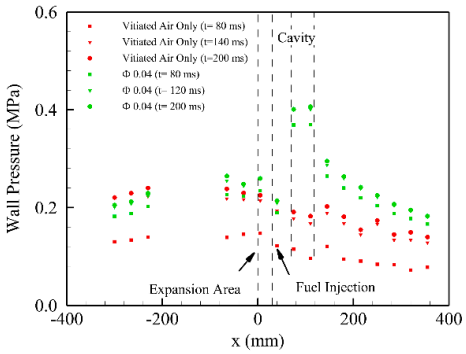

Figure 20. Wall pressure history of vitiated air and forced ignition.

Figure 21 shows the Schlieren snapshots of the scramjet combustor ignition and combustion process where the equivalence ratio (Φ) is 0.04. The images were captured at a resolution of 1280 × 208, exposure of 4 µs, and EDR (Extreme Dynamic Range) of 0.8 µs. The images were enhanced by +40% brightness and +40% contrast. (1) Fuel was injected into the scramjet combustor. As the air was not supplied, induced shock caused by a fuel jet wake was not formed. The fuel recirculation zone was created in the cavity. (2) GH_2 and GO_2 were ignited at VAH, and a high-temperature plume ignited the scramjet combustor fuel. The fuel jet wake and cavity leading edge induced slightly curved oblique shocks. The combustion area did not propagate into the cavity fuel recirculation zone, as the pressure of the upstream cavity did not surge, as shown in Figure 20. (3) Air was supplied into the VAH, and vitiated air was supplied into the scramjet combustor. The induced shock of the fuel jet wake was reflected between the bottom wall and the combustion area. The combustion area expanded into the cavity fuel recirculation zone. The flame between the fuel injector and the cavity leading edge moved downstream and lingered at the cavity leading edge. (4) The combustion area was confined in the cavity shear layer. The reflected oblique shocks were formed between the bottom wall and the combustion surface.

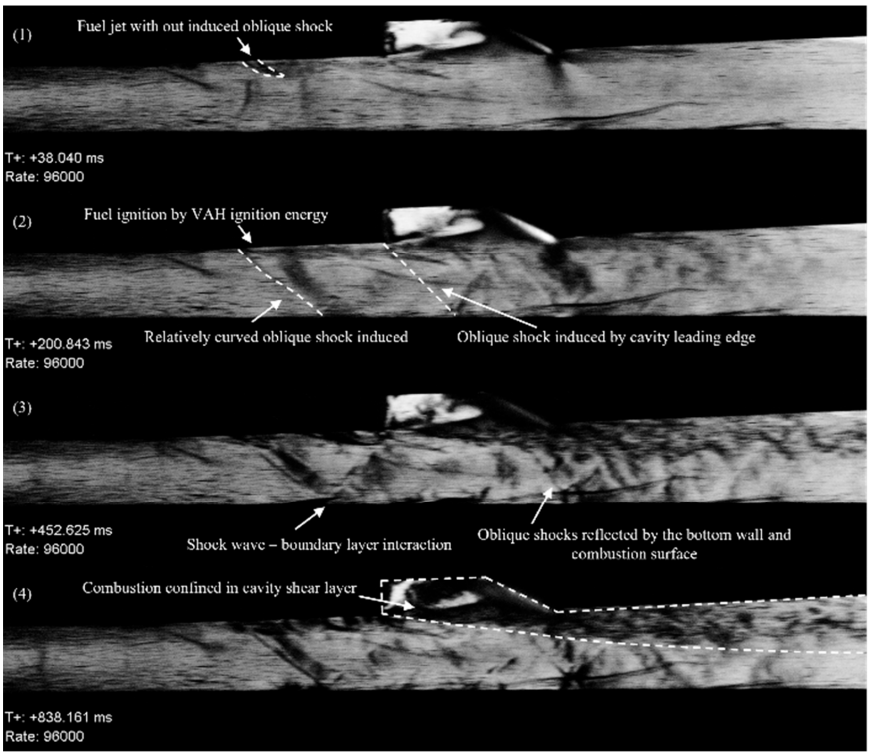

Figure 21. Schlieren snapshots of the scramjet combustor forced ignition at Φ = 0.04.

4. Conclusions

A rocket-type vitiation air heater was constructed and tested to supply high-enthalpy vitiated air to a direct-connect scramjet combustor. Room temperature GH_2, GO_2, and air were fed through pneumatic valves controlled by solenoid valves. A remote-controlled monitoring system was built for the auto-sequenced remote experiment. The air was supplied as the CWI ignited the GH_2 and GO_2, providing vitiated air to the scramjet combustor. The CRST nozzle, designed by the method of characteristics, was used for optimal cross-section transition and uniform flow feed. The nozzle exit Mach numbers at the top, middle, and bottom were measured using a tungsten wedge and θ-β-M relation. The Schlieren visualization method and a high-speed camera were used to capture the oblique shock induced by the wedges. The vitiated air was supplied at Mach 2.04 ± 0.04 into the scramjet combustor, and the total pressure was 1.685 ± 0.07 MPa, 2–3% of theoretical pressure calculated from the isentropic relation.

As the room-temperature GH_2 was not auto-ignited by the vitiated air, an additional ignition method was required. For a preliminary test for the ignitor, a forced ignition method was used to ignite the fuel, in which a high-temperature plume caused by VAH ignition ignited the scramjet combustor fuel. The pressure history showed that when only the vitiated air was supplied without fuel, the cavity pressure was 0.19 MPa. Therefore, an ignitor, such as a micro-pulse detonation engine, should exert higher pressure than the vitiated air under the cavity. Additionally, a high-speed camera captured Schlieren images of the ignition and combustion process. The cavity shear-layer combustion mode was formed in the scramjet combustor in Φ = 0.04, as shown in Figure 22. Therefore, the forced ignition method can be used as a reference model when the ignitor is used for the scramjet combustor.

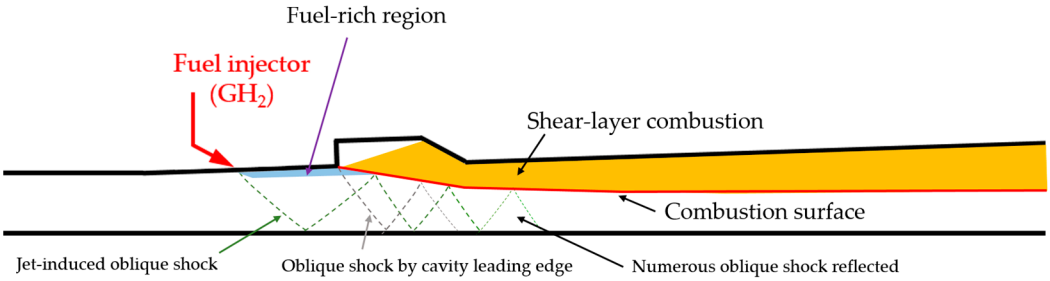

Figure 22. Schematic of the cavity shear-layer combustion mode at Φ = 0.04.

Author Contributions: Conceptualization, J.-Y.C.; methodology, H.-S.H., E.-S.L., J.-H.L., M.-S.K. and J.-Y.C.; software, E.-S.L.; writing—original draft preparation, J.-H.L.; writing—review and editing, M.-S.K. and J.-Y.C.; visualization, J.-H.L. and E.-S.L.; supervision, J.-Y.C.; project administration, J.-Y.C.; funding acquisition, J.-Y.C. All authors have read and agreed to the published version of the manuscript.

Funding: This research was supported by the Basic Research Program (No. 08-201-501-014) of the Agency for Defense Development (ADD), funded by the Defense Acquisition Program Administration (DAPA) of the Korean Government. Publication of this paper was supported by the BK21FOUR (Fostering Outstanding Universities for Research) program funded by the Ministry of Education (MOE, Korea) and National Research Foundation of Korea (NRF).

Institutional Review Board Statement: Not applicable.

Informed Consent Statement: Not applicable.

Data Availability Statement: Not applicable.

Conflicts of Interest: The authors declare no conflict of interest.

References

1. Liu, Q.; Baccarella, D.; Landsberg, W.; Veeraragavan, A.; Lee, T. Cavity Flameholding in an Optical Axisymmetric Scramjet in Mach 4.5 Flows. *Proc. Combust. Inst.* **2019**, *37*, 3733–3740. [CrossRef]
2. Baccarella, D.; Lui, Q.; Lee, T.; Hammack, S.D.; Do, H. The supersonic combustion facility ACT-2. In Proceedings of the 55th AIAA Aerospace Sciences Meeting, Grapevine, TX, USA, 9–13 January 2017. [CrossRef]
3. Vanyai, T.; Grieve, S.; Street, O.; Denman, Z.; Mclntyre, T.; Veeraragavan, A.; Smart, M. Fundamental scramjet combustiono experiments using hydrocarbon fuel. *J. Propuls. Power* **2019**, *35*, 953–963. [CrossRef]
4. Jeong, E.; O'Byrne, S.; Jeung, I.-S.; Houwing, A.F.P. The Effect of Fuel Injection Location on Supersonic Hydrogen Combustion in a Cavity-Based Model Scramjet Combustor. *Energies* **2020**, *13*, 193. [CrossRef]
5. Garrard, D.; Bates, B.; Rigney, S. Progress Report on the APTU Upgrade Activities. In Proceedings of the 24th AIAA Aerodynamic Measurement Technology and Ground Testing Conference, Portland, OR, USA, 28 June–1 July 2004; American Institute of Aeronautics and Astronautics: Reston, VA, USA, 2004.
6. Meng, Y.; Gu, H.; Zhuang, J.; Sun, W.; Gao, Z.; Lian, H.; Yue, L.; Chang, X. Experimental Study of Mode Transition Characteristics of a Cavity-Based Scramjet Combustor during Acceleration. *Aerosp. Sci. Technol.* **2019**, *93*, 105316. [CrossRef]
7. Zhang, J.; Chang, J.; Wang, Z.; Gao, L.; Bao, W. Flame Propagation and Flashback Characteristics in a Kerosene Fueled Supersonic Combustor Equipped with Strut/Wall Combined Fuel Injectors. *Aerosp. Sci. Technol.* **2019**, *93*, 105303. [CrossRef]
8. Peng, J.; Cao, Z.; Yu, X.; Yang, S.; Yu, Y.; Ren, H.; Ma, Y.; Zhang, S.; Chen, S.; Zhao, Y. Analysis of Combustion Instability of Hydrogen Fueled Scramjet Combustor on High-Speed OH-PLIF Measurements and Dynamic Mode Decomposition. *Int. J. Hydrogen Energy* **2020**, *45*, 13108–13118. [CrossRef]
9. Tian, Y.; Yang, S.; Le, J.; Su, T.; Yue, M.; Zhong, F.; Tian, X. Investigation of Combustion and Flame Stabilization Modes in a Hydrogen Fueled Scramjet Combustor. *Int. J. Hydrogen Energy* **2016**, *41*, 19218–19230. [CrossRef]
10. Nishimoto, S.; Nakaya, S.; Lee, J.; Tsue, M. Effects of the Penetration Height of Ethylene Transverse Jets on Flame Stabilization Behavior in a Mach 2 Supersonic Crossflow. *Proc. Combust. Inst.* **2022**, in press. [CrossRef]
11. Wang, Z.; Sun, M.; Wang, H.; Yu, J.; Liang, J.; Zhuang, F. Mixing-Related Low Frequency Oscillation of Combustion in an Ethylene-Fueled Supersonic Combustor. *Proc. Combust. Inst.* **2015**, *35*, 2137–2144. [CrossRef]
12. Yuan, Y.; Zhang, T.; Yao, W.; Fan, X.; Zhang, P. Characterization of Flame Stabilization Modes in an Ethylene-Fueled Supersonic Combustor Using Time-Resolved CH* Chemiluminescence. *Proc. Combust. Inst.* **2017**, *36*, 2919–2925. [CrossRef]
13. Zhang, J.; Chang, J.; Ma, J.; Wang, Y.; Bao, W. Investigations on Flame Liftoff Characteristics in Liquid-Kerosene Fueled Supersonic Combustor Equipped with Thin Strut. *Aerosp. Sci. Technol.* **2019**, *84*, 686–697. [CrossRef]
14. Li, F.; Sun, M.; Cai, Z.; Sun, Y.; Li, F.; Zhang, J.; Zhu, J. Experimental Study of Flame Stabilization in a Single-Side Expansion Scramjet Combustor with Different Cavity Length-to-Depth Ratios. *Acta Astronaut.* **2020**, *173*, 1–8. [CrossRef]
15. An, B.; Sun, M.; Wang, Z.; Chen, J. Flame Stabilization Enhancement in a Strut-Based Supersonic Combustor by Shock Wave Generators. *Aerosp. Sci. Technol.* **2020**, *104*, 105942. [CrossRef]
16. Nakaya, S.; Yamana, H.; Tsue, M. Experimental Investigation of Ethylene/Air Combustion Instability in a Model Scramjet Combustor Using Image-Based Methods. *Proc. Combust. Inst.* **2021**, *38*, 3869–3880. [CrossRef]
17. Yang, P.; Xia, Z.; Ma, L.; Chen, B.; Feng, Y.; Zhang, J. Experimental Study on the Influence of the Injection Structure on Solid Scramjet Performance. *Acta Astronaut.* **2021**, *188*, 229–238. [CrossRef]
18. Yu, K.; Su, P.; Chen, Y.; Xu, J. Inverse Design of flow Distortion Dominated by Shock Wave Interaction with Experimental Verification. *Int. J. Aeronaut. Space Sci.* **2021**, *22*, 866–873. [CrossRef]
19. Gordon, S.; McBride, B.J. *Computer Program for Calculation of Complex Chemical Equilibrium Compositions and Applications. Part 1: Analysis*; No. NAS 1.61: 1311; NASA: Cleveland, OH, USA, 1994.
20. Marshall, W.; Pal, S.; Woodward, R.; Santoro, R. Benchmark wall heat flux data for a GO2/GH2 single element combustor. In Proceedings of the 41st AIAA/ASME/SAE/ASEE Joint Propulsion Conference & Exhibit, Tuscon, AZ, USA, 10–13 July 2005. [CrossRef]
21. Sung, B.-K.; Choi, J.-Y. Design of a Mach 2 Shape Transition Nozzle for Lab-Scale Direct-Connect Supersonic Combustor. *Aerosp. Sci. Technol.* **2021**, *117*, 106906. [CrossRef]
22. Sung, B.-K.; Jeong, S.-M.; Choi, J.-Y. Direct-Connect Supersonic Nozzle Design Considering the Effect of Combustion. *Aerosp. Sci. Technol.* **2023**, *133*, 108094. [CrossRef]
23. Han, H.-S.; Kim, J.-M.; Oh, S.; Choi, J.-Y. An Experimental Study on Characteristics of Small-scale PDE under Low-frequency Operating Conditions. *J. Korean Soc. Propuls. Eng.* **2018**, *22*, 81–89. [CrossRef]